Test–Retest Reliability of the SERT Imaging Agent 11C-HOMADAM in Healthy Humans

Vikram Adhikarla[1], Boadie W. Dunlop[2], Nashwa Jarkas[1], Mark M. Goodman[1,2], Helen Mayberg[2], Michael J. Owens[2], and Jonathon A. Nye[1]

[1]*Department of Radiology and Imaging Sciences, Emory University, Atlanta, Georgia; and* [2]*Department of Psychiatry and Behavioral Sciences, Emory University, Atlanta, Georgia*

The aim of this study was to measure the test–retest reliability of 11C-*N,N*-dimethyl-2-(2′-amino-4′-hydroxymethylphenylthio)benzylamine (11C-HOMADAM) imaging of serotonin transporter (SERT) density in healthy control subjects. **Methods:** Two female and 2 male volunteers participated in the study, with each undergoing three 90-min 11C-HOMADAM PET scans. Time–activity curves were derived from SERT-rich structures and fit to 2 models: a simplified reference tissue model and a multilinear graphical model. Binding potential, the ratio of specifically bound uptake to nondisplaceable uptake at equilibrium, was calculated from the model parameter estimates. Ninety-five percent confidence intervals and the intraclass correlation coefficient (ICC) were calculated and adjusted for repeated measures. **Results:** The ICC values ranged from −0.13 in the dorsal raphe to 0.88 in the caudate nucleus. The highest average ICC values were in the striatum, but other regions were sensitive to measurement outliers. **Conclusion:** Good-to-excellent test–retest reliability was observed for SERT binding in the striatum. The dorsal raphe ICC value was sensitive to a measurement outlier. 11C-HOMADAM binding potential calculated from the simplified reference tissue model and the multilinear graphical model were robust and in good agreement.

Key Words: serotonin transporter; 11C-HOMADAM; test–retest; binding potential; positron emission tomography

Altered serotonin (5-HT) neurotransmission has been associated with a variety of neurologic and behavioral disorders (*1*). Of particular interest is the role of the serotonin transporter (SERT) in mediating serotonin availability and the role of SERT as the primary target for several antidepressant medications (*2*). Mapping the SERT distribution in the brain with PET permits evaluation of SERT availability and integrity. In addition, the availability of SERT under an altered state can be imaged to assess pharmacologic treatments, assist in developing psychiatric medications, and further the understanding of psychiatric illness (*3,4*).

To measure SERT density in vivo, our group developed 11C-*N, N*-dimethyl-2-(2′-amino-4′-hydroxymethylphenylthio)benzylamine (11C-HOMADAM), a highly specific SERT imaging agent showing fast uptake kinetics and negligible binding in the cerebellum (*5*). Measurement of SERT density with 11C-HOMADAM was characterized in healthy humans with a 3-parameter reference tissue model (*6*). In a group comparison or longitudinal study, knowledge of the test-to-test variability over time is desired to estimate the minimum detectable change for a given population size. One interest in neuroimaging is optimization of drug dosage and delivery, with baseline and drug challenge PET acquisitions being performed to derive an estimate of SERT occupancy. The aim of this study was to measure the test–retest reliability of 11C-HOMADAM in healthy control subjects using a 3-scan test–retest protocol.

MATERIALS AND METHODS

Human Subjects

This study was conducted under the auspices of the Emory Internal Review Board and within the Emory University Hospital. Two female and 2 male volunteers (mean age ± SD, 24 ± 2 y) participated in the study after giving informed consent. All subjects were considered physically and mentally healthy as judged by the absence of any history of neurologic or psychiatric (including substance abuse) disorders and the absence of any active medical conditions. All subjects underwent a physical examination, electrocardiogram, and laboratory testing of blood and urine samples. No subjects were taking medications known to bind to the SERT.

MRI

MR images were collected on an Avanto Magnetom 1.5-T scanner (Siemens Medical Solutions) with a 16-channel receiver array head coil. A standard whole-brain T1-weighted magnetization-prepared rapid-acquisition gradient-echo sequence was acquired for anatomic reference and to aid in delineating regions of interest (ROIs) on PET images (*7*). The scan parameters were 5-mm-thick 2-dimensional T1-weighted images with a transverse plane pixel size of 0.72 mm (repetition time/echo time, 430/17 ms; flip angle, 90°; acquisition field of view, 320 × 192 pixels; matrix, 320 × 320 pixels).

Radiochemistry

11C-HOMADAM was synthesized by methylation of *N*-methyl-2-(2′-amino-4′-hydroxymethylphenylthio)benzylamine with 11C-CH$_3$I as previously described (*5*). The radiochemical purity of 11C-HOMADAM was more than 98%, with an average specific activity of 19.4 ± 4.6 GBq/μmol.

PET Protocol

PET scans were performed on a Siemens High-Resolution Research Tomograph: a 3-dimensional dual-layer lutetium oxyorthosilicate and lutetium-yttrium oxyorthosilicate detector system with depth-of-interaction discrimination and an isotropic in-plane resolution of 2.2 mm in full

width at half maximum. The subjects were positioned supine, with head movement constrained by a rigid head cradle and strap restraints. A venous catheter was prepared in one of the forearms for injection of the radiopharmaceutical. Before the emission study, a 6-min transmission scan with ^{137}Cs was acquired for attenuation correction. The subjects underwent 3 ^{11}C-HOMADAM PET scans separated by 1–2 wk. Each emission scan was a 90-min acquisition started at the beginning of an infusion of ^{11}C-HOMADAM delivered over a duration of 5 min using a syringe pump. The data were collected in list mode and later histogrammed into 18 frames (6 × 30 s, 4 × 180 s, and 8 × 600 s).

PET emission data were corrected for attenuation, randoms, and scatter and reconstructed with an ordinary Poisson ordered-subset expectation-maximization algorithm (6 iterations and 16 subsets) to a 256 × 256 × 207 image matrix (voxel size, 1.2 mm³) (8,9). Image data were smoothed after reconstruction with a gaussian filter of 4 mm in full width at half maximum to reduce noise and improve contrast in the brain stem. The final isotropic resolution was 4.6 mm and matched that reported in our previous work (6).

Image Analysis and Derivation of SERT Availability

Each reconstructed dynamic image frame was coregistered to its neighbor and aligned to a reference frame using the mutual-information metric (10,11). The test and 2 retest images were then aligned to one another and lastly to the subject's MR images using the same metric. Summed image data from the first acquisition were created between 10 and 45 min to assist with region drawing. ROIs ($n = 11$) were drawn manually on the coregistered transaxial and sagittal MR images within anatomic boundaries using software that we developed in the Interactive Data Language environment (ITT Corp.). ROIs included the SERT-rich structures of the midbrain, red nucleus, dorsal raphe, pulvinar thalamus, putamen, caudate nucleus, and amygdala and the SERT-poor areas of the cingulate cortex, prefrontal cortex, inferior occipital cortex, and pons. The red nucleus, midbrain, and dorsal raphe could not be delineated on MR images because of a lack of contrast defining their boundaries. Instead, these structures were delineated on each subject's summed test PET images (first PET) in the sagittal plane, which exhibited distinct focal uptake. An additional ROI was drawn bilaterally on the cerebellar crus and served as a reference tissue for calculation of SERT density in the kinetic modeling. All ROIs were transferred to each frame of the dynamic PET data to generate time–activity curves used to derive the SERT binding parameters. Bilateral structures were averaged.

^{11}C-HOMADAM binding to the SERT was estimated by fitting the time–activity curve data to a reference tissue compartmental model (12). Previous work by our group showed that the reference-model approach best approximated ^{11}C-HOMADAM time–activity data when fit using a single target-tissue compartment, or 3 parameters (R, k_2, and k_{2a}) (6), described as the simplified reference tissue model (SRTM) (13) and arranged in the following operational form:

$$C_t = RC_r(t) + R(k_2 - k_{2a})C_t(t) \ast e^{-k_{2a}t}, \qquad \text{Eq. 1}$$

where * represents the convolution operator. In this compartment model, C_r represents the reference tissue compartment and C_t represents the target ROI, where the free and specific compartments were not distinguishable from one another. The unidirectional rate constants representing the influx of the radioligand from the blood plasma to the target region, K_1, and reference region, K_1', enter the compartment equations as a ratio, $R = K_1/K_1'$. Therefore, R and the efflux rate constants to blood plasma from the target, k_2, and reference region, k_{2a}, were estimated simultaneously by fitting Equation 1 to the measured time–activity curves using the Powell minimization routine (14) in the Interactive Data Language environment.

In the compartment model, SERT density was calculated by correcting the regional distribution volumes for nondisplaceable uptake calculated from the cerebellum ROI (15). This correction assumes that nondisplaceable uptake does not vary significantly among regions and that the negligibly low SERT expression in the cerebellum represents only nondisplaceable uptake (16–18). On the basis of these assumptions, the binding potential, BP_{ND} (the ratio of specifically bound uptake to nondisplaceable uptake at equilibrium), can be calculated for each region as follows:

$$BP_{ND} = \frac{f_{ND}B_{avail}}{K_d} = \left[R\frac{k_{2a}}{k_2} \right] - 1, \qquad \text{Eq. 2}$$

where f_{ND} represents the free fraction of radioligand in the nondisplaceable tissue, B_{avail} (nmol/L) represents the number of available binding sites, and K_d (nmol/L) represents the equilibrium dissociation constant. It was further assumed that the free fraction of radioligand does not vary between subject groups, permitting direct comparison of BP_{ND}.

In the application of graphical models to our previous dataset, the Logan method produced biased reductions in BP_{ND} caused by the presence of the noisy-target-tissue radioactivity term, $C_t(T)$, on both the left and the right sides of the equation (19,20). To address the noise-induced bias, the graphical multilinear reference tissue model (MRTM) (21) was applied to the time–activity data using the operational form in which $C_t(T)$ does not present with the dependent variables (22),

$$C_t(T) = -\frac{DVR}{b}\int_0^T C_r(t)dt + \frac{1}{b}\int_0^T C_t(t)dt - \frac{DVR}{k_{2a}b}C_r(t), \qquad \text{Eq. 3}$$

where DVR represents the distribution volume ratio of the target to reference tissue ($BP_{ND} + 1$) and $-1/b$ represents k_2, the efflux rate constant to plasma from the target. The above equation decreases noise-induced bias and does not require assignment of compartments or initial parameter guesses. Since ^{11}C-HOMADAM can be represented using a single tissue model, the graphically transformed regression data become linear starting at $T = 0$ and the distribution volume ratio may be calculated by the division of the first and second linear coefficients.

Statistical Analysis

Data are expressed as mean with SD. Brain-region mean BP_{ND} and 95% confidence intervals were estimated using an unconditional-means random-effects model in which the subjects were entered as random effects. This model adjusts variances for the presence of correlated data due to repeatedly measured subjects. Using this modeling, we also estimated the intraclass correlation coefficient (ICC), the ratio of between-subject variance to total variance (between-subject plus residual variance) (23),

$$ICC = \frac{MSBS - MSWS}{MSBS + (k - 1)MSWS}, \qquad \text{Eq. 4}$$

where $MSBS$ and $MSWS$ are the mean sum of squares between and within subjects, and k is the number of repeated subject measurements. This ICC is a measure of reliability of the BP_{ND} measure when the measurement time points have no intrinsic meaning; higher values indicate greater reliability. An ICC value of below 0.4 is considered poor; a value of 0.40–0.59, fair; a value of 0.60–0.74, good; and a value of above 0.75, excellent (24). Analyses were performed with SAS software (version 9.2; SAS Institute Inc.).

RESULTS

Table 1 lists the patient demographics and duration in days between a subject's first PET scan and each of the 2 retest PET

TABLE 1
Patient Demographics and Test–Retest Timing

Subject no.	Age (y)	Sex	Days from initial test to first retest	Days from initial test to second retest
1	24	M	28	42
2	26	M	7	14
3	24	F	19	40
4	21	F	21	35
Mean ± SD	24 ± 2		19 ± 9	33 ± 13

scans. The average activity administered was 677 ± 96 MBq, with a range of 507–800 MBq. The average specific activity at the time of injection was 19.4 MBq/μmol, with a range of 14.7–30.5 MBq/μmol. Figure 1 shows summed images from 10 to 45 min in the first test PET scan and ROI definitions overlaid on the MR image for subject 3. There was a rapid increase of ^{11}C-HOMADAM into the brain, peaking at 20 min in SERT-rich regions with the exception of the midbrain, which peaked at 35 min. The cerebellum had the lowest radioactivity concentration in all subject scans.

The mean regional BP_{ND} values agreed well between the SRTM and MRTM models (Tables 2 and 3). Ninety-five percent confidence intervals were narrow in regions of high SERT density and gradually increased in regions of low SERT density. The ICC values ranged from -0.17 in the dorsal raphe to 0.88 in the caudate nucleus. Excellent ICC values were found in the striatal structures, anterior cingulate, pons, and frontal cortex. ICCs in the midbrain,

FIGURE 1. (Top) Representative subject MRI superimposed with ROIs used to generate time–activity curves. (Bottom) Corresponding PET images of summed ^{11}C-HOMADAM uptake from 55 to 90 min fused with MR image data. Elevated uptake was observed in SERT-rich structures of midbrain, pulvinar thalamus, and striatum. Cerebellum had lowest uptake over imaging timecourse and was used as reference region in compartmental analysis.

thalamic structures, raphe chain, and other cortical areas were more variable and did not show a decreasing trend with SERT density.

DISCUSSION

The objective of this study was to evaluate the test–retest reliability of ^{11}C-HOMADAM binding to the SERT in healthy subjects using a reference model approach. We were interested in the repeated test variability for deriving dose occupancy curves using a 3-injection protocol. The structure of interest in assessing pharmacologic response was the striatum, which is large and can be reliably delineated on MRI T1-weighted contrast-enhanced images. Using the SRTM model to estimate BP_{ND}, we found good reliability in the putamen and excellent reliability in the caudate. Additionally, we found similarly robust reliability for the MRTM graphical approach, which addresses the noise-induced reduction of BP_{ND} previously shown with the Logan graphical model in the original validation of ^{11}C-HOMADAM (6).

In the test and first retest, the BP_{ND} in the dorsal raphe nucleus did not follow the expected rank order of dorsal raphe > midbrain > pulvinar thalamus > striatum observed in postmortem studies (16–18) or in our previous study (6). The dorsal raphe nucleus is a small subnucleus of the raphe chain (i.e., dorsal, magnus, and pallidus raphe), with the largest number of serotonergic neurons, but it cannot be identified on T1-weighted structural MR images and was instead delineated on each subject's test PET images and then copied to the first and second retest PET images. A combination of differences in delineation of the dorsal raphe ROI between subjects, the less favorable imaging statistics of the small region, and the partial-volume effect may have contributed to the lower BP_{ND} mean value for the dorsal raphe than for the midbrain. The ROI analysis overall was not sensitive to local foci contained within the region, which would be more appropriately examined with a parametric analysis approach.

The ICC reliability measure varied considerably by region in SERT-rich structures and ranged from poor reliability in the brain stem structures to excellent reliability in the caudate nucleus. Because of the small number of subjects, the ICC values were sensitive to measurement outliers. These outliers reduced the estimation reliability in the SERT-rich structures of the dorsal raphe. Negative values should be considered to be due to sampling error and to be equivalent to having no reliability. The negative ICC value for the dorsal raphe from the SRTM model can be explained in part by a strong outlier in the second retest study of subject 2. Removing this outlier from the ICC calculation raised the ICC value in the dorsal raphe to 0.12. Similarly, removing the same outlier from the MRTM modeling results raised the ICC value to 0.33. It can be concluded that the poor reliability observed in the brain stem structures after correction for outliers has model dependence and also indicates a high within-subject coefficient of variation, as this contributes to lower ICC values as defined by Equation 4.
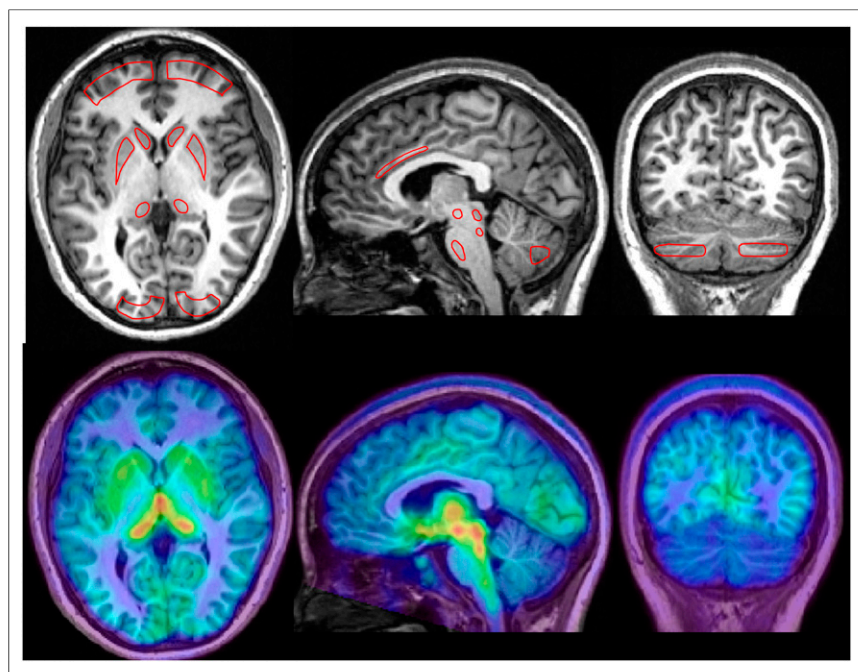
TABLE 2
Regional BP$_{ND}$ Values for ^{11}C-HOMADAM Test–Retest–Retest Calculated Using SRTM

Region	ROI volume (mm^3)	Test	First retest	Second retest	Mean BP$_{ND}$	ICC
Midbrain	499 ± 96	4.03 ± 0.50	3.52 ± 0.33	3.75 ± 0.55	3.77 (3.15, 4.38)	0.40
Dorsal raphe	245 ± 28	3.50 ± 0.13	3.30 ± 0.17	3.95 ± 0.79	3.58 (3.11, 4.05)	−0.17
Red nucleus	302 ± 48	3.85 ± 0.53	3.35 ± 0.08	3.45 ± 0.47	3.55 (3.03, 4.07)	0.32
Pulvinar thalamus	744 ± 73	2.69 ± 0.25	2.43 ± 0.13	2.50 ± 0.23	2.54 (2.23, 2.84)	0.50
Amygdala	729 ± 28	1.85 ± 0.34	1.60 ± 0.18	1.83 ± 0.50	1.76 (1.26, 2.25)	0.57
Putamen	1,271 ± 41	1.73 ± 0.29	1.57 ± 0.24	1.68 ± 0.32	1.66 (1.24, 2.08)	0.73
Caudate nucleus	678 ± 129	1.53 ± 0.38	1.43 ± 0.26	1.39 ± 0.26	1.45 (0.98, 1.91)	0.88
Cingulate cortex	972 ± 261	0.56 ± 0.15	0.53 ± 0.09	0.60 ± 0.25	0.56 (0.31, 0.82)	0.78
Pons	575 ± 254	0.56 ± 0.19	0.52 ± 0.10	0.50 ± 0.18	0.53 (0.28, 0.77)	0.83
Inferior occipital cortex	1,460 ± 312	0.48 ± 0.12	0.44 ± 0.08	0.59 ± 0.34	0.50 (0.28, 0.73)	0.19
Prefrontal cortex	3,195 ± 1,126	0.23 ± 0.09	0.16 ± 0.08	0.21 ± 0.11	0.20 (0.06, 0.35)	0.78

Data in parentheses are 95% confidence intervals adjusted for multiple observations per subject.

Larger SERT-poor structures such as the prefrontal cortex, cingulate cortex, and pons had excellent reliability. In contrast, the inferior occipital cortex was not consistent with these SERT-poor regions even though its ROI volume was large and should have benefited from better sampling statistics. The poor reliability of the occipital cortex can be largely explained by a measurement outlier, whose removal increased the ICC value to 0.61 with SRTM and 0.63 with MRTM.

Comparisons can be made between the ICC values for ^{11}C-HOMADAM and those for other SERT imaging agents. Two groups reported excellent ^{11}C-DASB ICC values of 0.86 (25) and 0.89 (26) in the striatum but did not distinguish between the caudate and putamen. The ^{11}C-DASB ICC value for the frontal cortex was reported to be 0.65 by Frankle et al. (25) and was lower than that calculated in the current work, although the fact that the ROI volumes are not known could complicate a direct comparison. ^{11}C-DASB ICC values from SERT-rich structures of the brain stem are more complicated to compare with ^{11}C-HOMADAM ICC values. Frankle et al. (25) reported a midbrain ICC of 0.82 that included a portion of the raphe chain signal because of the limited resolution of the PET camera, and Kim et al. (26) delineated only the raphe (ICC, 0.39) although it is unknown which subnuclei were contained within the ROI.

The reported ICC values for the structurally similar diphenyl sulfide derivative ^{11}C-MADAM were only fair in the striatum (putamen) (ICC, 0.55) and raphe nuclei (ICC, 0.55) but excellent in the frontal cortex (ICC, 0.96) (27). The administered activity reported for ^{11}C-MADAM was approximately half (298–313 MBq) that reported in the current work (677 ± 96 MBq), resulting in a lower overall activity concentration in the brain, which could contribute to the lower ICC values of the putamen and raphe nuclei. It has been suggested by Parsey et al. (28) that an ICC value above 0.5 is acceptable for repeat analysis of PET and that a value above 0.75 is excellent. Therefore, the ^{11}C-HOMADAM ICC values of SERT-rich structures of the midbrain, red nucleus,

TABLE 3
Regional BP$_{ND}$ Values for ^{11}C-HOMADAM Test–Retest–Retest Calculated Using MRTM

Region	ROI volume (mm^3)	Test	First retest	Second retest	Mean BP$_{ND}$
Midbrain	4.08 ± 0.60	3.52 ± 0.33	3.75 ± 0.56	3.78 (3.10, 4.47)	0.45
Dorsal raphe	3.72 ± 0.26	3.29 ± 0.17	3.90 ± 0.75	3.64 (3.12, 4.15)	0.12
Red nucleus	3.81 ± 0.54	3.32 ± 0.07	3.45 ± 0.48	3.52 (2.99, 4.05)	0.33
Pulvinar thalamus	2.67 ± 0.24	2.42 ± 0.12	2.48 ± 0.23	2.52 (2.23, 2.81)	0.50
Amygdala	1.81 ± 0.35	1.59 ± 0.17	1.81 ± 0.48	1.73 (1.25, 2.22)	0.57
Putamen	1.70 ± 0.28	1.57 ± 0.24	1.67 ± 0.32	1.65 (1.24, 2.05)	0.72
Caudate nucleus	1.51 ± 0.38	1.42 ± 0.25	1.38 ± 0.25	1.44 (0.97, 1.90)	0.88
Cingulate cortex	0.54 ± 0.13	0.52 ± 0.08	0.59 ± 0.25	0.55 (0.31, 0.79)	0.74
Pons	0.55 ± 0.18	0.52 ± 0.10	0.50 ± 0.18	0.52 (0.28, 0.76)	0.83
Inferior occipital cortex	0.50 ± 0.15	0.44 ± 0.08	1.13 ± 1.42	0.69 (−0.12, 1.50)	0.07
Prefrontal cortex	0.22 ± 0.09	0.16 ± 0.08	0.21 ± 0.11	0.20 (0.05, 0.34)	0.80

Data in parentheses are 95% confidence intervals adjusted for multiple observations per subject.

and dorsal raphe would not have sufficiently high ICC values to reliably measure BP_{ND}.

The ability to reliably measure SERT has significant applications for assessing important issues in drug development, including effective central nervous system penetration of drugs and dose–response relationships. Furthermore, quantifying SERT density may have value in understanding the pathophysiology of psychiatric illness and in predicting response to treatments that target the SERT. The small number of subjects analyzed in this report presents some limitations, as noted above regarding sensitivity to measurement outliers. However, our goal is to use ^{11}C-HOMADAM to assess occupancy of selective serotonin reuptake inhibitors, and the presented data show that the striatal structures serve as a reliable measure of SERT density in the brain for this purpose.

CONCLUSION

Good-to-excellent test–retest reliability for SERT binding in serotonergic-rich areas of the striatum was observed with ^{11}C-HOMADAM imaging. SRTM and MRTM modeling yielded BP_{ND} values in strong agreement, with the same rank orders and well-matched ICC values.

DISCLOSURE

ACKNOWLEDGMENT

REFERENCES

1. Barnes NM, Sharp T. A review of central 5-HT receptors and their function. *Neuropharmacology.* 1999;38:1083–1152.
2. Owens MJ, Nemeroff CB. Role of serotonin in the pathophysiology of depression: focus on the serotonin transporter. *Clin Chem.* 1994;40:288–295.
3. Laruelle M, Slifstein M, Huang Y. Positron emission tomography: imaging and quantification of neurotransmitter availability. *Methods.* 2002;27:287–299.
4. Guilloteau D, Chalon S. PET and SPECT exploration of central monoaminergic transporters for the development of new drugs and treatments in brain disorders. *Curr Pharm Des.* 2005;11:3237–3245.
5. Jarkas N, Votaw JR, Voll RJ, et al. Carbon-11 HOMADAM: a novel PET radiotracer for imaging serotonin transporters. *Nucl Med Biol.* 2005;32:211–224.
6. Nye JA, Votaw JR, Jarkas N, et al. Compartmental modeling of ^{11}C-HOMADAM binding to the serotonin transporter in the healthy human brain. *J Nucl Med.* 2008;49:2018–2025.
7. Mugler JP III. Overview of MR imaging pulse sequences. *Magn Reson Imaging Clin N Am.* 1999;7:661–697.
8. van Velden FH, Kloet RW, van Berckel BN, Wolfensberger SPA, Lammertsma AA, Boellaard R. Comparison of 3D-OP-OSEM and 3D-FBP reconstruction algorithms for High-Resolution Research Tomograph studies: effects of randoms estimation methods. *Phys Med Biol.* 2008;53:3217–3230.
9. Comtat C, Bataille F, Michel C, et al. OSEM-3D reconstruction strategies for the ECAT HRRT. *IEEE Nucl Sci Symp Conf Rec.* 2004;6:3492–3496.
10. Maes F, Collignon A, Vandermeulen D, Marchal G, Suetens P. Multimodality image registration by maximization of mutual information. *IEEE Trans Med Imaging.* 1997;16:187–198.
11. Herzog H, Tellmann L, Fulton R, et al. Motion artifact reduction on parametric PET images of neuroreceptor binding. *J Nucl Med.* 2005;46:1059–1065.
12. Lammertsma AA, Bench CJ, Hume SP, et al. Comparison of methods for analysis of clinical [11C]raclopride studies. *J Cereb Blood Flow Metab.* 1996;16:42–52.
13. Lammertsma AA, Hume SP. Simplified reference tissue model for PET receptor studies. *Neuroimage.* 1996;4:153–158.
14. Press WH. *Numerical Recipes: The Art of Scientific Computing.* New York, NY: Cambridge University Press; 1989.
15. Innis RB, Cunningham VJ, Delforge J, et al. Consensus nomenclature for in vivo imaging of reversibly binding radioligands. *J Cereb Blood Flow Metab.* 2007;27:1533–1539.
16. Bäckström I, Bergstrom M, Marcusson J. High affinity [3H]paroxetine binding to serotonin uptake sites in human brain tissue. *Brain Res.* 1989;486:261–268.
17. Cortés R, Soriano E, Pazos A, Probst A, Palacios JM. Autoradiography of antidepressant binding sites in the human brain: localization using [3H]imipramine and [3H]paroxetine. *Neuroscience.* 1988;27:473–496.
18. Laruelle M, Vanisberg MA, Maloteaux JM. Regional and subcellular localization in human brain of [3H]paroxetine binding, a marker of serotonin uptake sites. *Biol Psychiatry.* 1988;24:299–309.
19. Ichise M, Toyama H, Innis RB, Carson RE. Strategies to improve neuroreceptor parameter estimation by linear regression analysis. *J Cereb Blood Flow Metab.* 2002;22:1271–1281.
20. Slifstein M, Laruelle M. Effects of statistical noise on graphic analysis of PET neuroreceptor studies. *J Nucl Med.* 2000;41:2083–2088.
21. Ichise M, Ballinger JR, Golan H, et al. Noninvasive quantification of dopamine D2 receptors with iodine-123-IBF SPECT. *J Nucl Med.* 1996;37:513–520.
22. Ichise M, Liow JS, Lu JQ, et al. Linearized reference tissue parametric imaging methods: application to [11C]DASB positron emission tomography studies of the serotonin transporter in human brain. *J Cereb Blood Flow Metab.* 2003;23:1096–1112.
23. Shrout PE, Fleiss JL. Intraclass correlations: uses in assessing rater reliability. *Psychol Bull.* 1979;86:420–428.
24. Cicchetti DV. Guidelines, criteria, and rules of thumb for evaluating normed and standardized assessment instruments in psychology. *Psychol Assess.* 1994;6:284–290.
25. Frankle WG, Slifstein M, Gunn RN, et al. Estimation of serotonin transporter parameters with ^{11}C-DASB in healthy humans: reproducibility and comparison of methods. *J Nucl Med.* 2006;47:815–826.
26. Kim JS, Ichise M, Sangare J, Innis RB. PET imaging of serotonin transporters with [11C]DASB: test-retest reproducibility using a multilinear reference tissue parametric imaging method. *J Nucl Med.* 2006;47:208–214.
27. Lundberg J, Halldin C, Farde L. Measurement of serotonin transporter binding with PET and [11C]MADAM: a test-retest reproducibility study. *Synapse.* 2006;60:256–263.
28. Parsey RV, Slifstein M, Hwang DR, et al. Validation and reproducibility of measurement of 5-HT1A receptor parameters with [carbonyl-11C]WAY-100635 in humans: comparison of arterial and reference tissue input functions. *J Cereb Blood Flow Metab.* 2000;20:1111–1133.